21st Australasian Fluid Mechanics Conference
Adelaide, Australia
10-13 December 2018

Lift and Drag forces on a particle near a wall at low Reynolds numbers

Nilanka I. K. Ekanayake[1], Joseph D. Berry[1], Anthony D. Stickland[1], Ineke L. Muir[2], Steven K. Dower[2] and Dalton J. E. Harvie[1]

[1]Department of Chemical Engineering, The University of Melbourne, Victoria 3010 Australia.

[2]CSL, Bio21 Molecular Science and Biotechnology Institute, Victoria 3052, Australia.

Abstract

Shear induced lift and drag forces on a small, neutrally buoyant, rigid spherical particle, moving close to a wall ($l/a = 1.2$) are examined. These wall induced forces are computed numerically in a linear flow for low particle and shear Reynolds numbers ($Re_p \leq 1$ & $Re_\gamma \leq 1$). Mesh resolution and domain size dependencies for low Reynolds numbers are examined. Decomposed slip and shear hydrodynamic forces are analysed separately for a fixed and moving particle. Numerical results are compared with theoretically predicted forces for $Re_\gamma, Re_p \ll 1$. The deviations of lift forces from theoretical values demonstrate a strong shear rate dependence near the wall for finite Re_γ values. Results presented will aid in developing a comprehensive wall-induced lift model valid for a range of finite Reynolds numbers to analyze the cross stream migration of particles in wall bounded flows.

Introduction

Hydrodynamic forces acting on a particle moving in a shear flow close to a wall are significant in industrial and medical applications such as, cancer-detecting and cell sorting in microfluidics, and in flow cytometery [1]. In the biological flow context, wall induced forces contribute to the separation between platelets and red blood cells that results in a Cell Free Layer (CFL) forming adjacent to blood vessel walls. CFL development is crucial for blood clot formation, as the presence of this layer increases the platelet concentration near (damaged) vasculature walls, enhancing the coagulation rates [2].

Cross stream migration of particles in dilute suspension flow is primarily caused by lift forces. Lift is an inertia induced force that reduces to zero in the Stokes limit. In unbounded flow, a neutrally buoyant particle can experience lift due to slip (relative particle velocity), combined with shear or rotation [3, 4]. Near a wall, the presence of the wall induces extra flow disturbances, resulting in increased lift forces. Theoretical models of wall induced lift have mainly been developed via the the method of matched asymptotic expansion. These analyses are restricted to very low inertia conditions (low particle Reynolds number $Re_p = u_{slip}a/\nu \ll 1$ and shear Reynolds number $Re_\gamma = \gamma a^2/\nu \ll 1$), where a, u_{slip}, γ and ν are the particle radius, slip velocity, shear rate and fluid kinetic viscosity respectively. The lift forces are computed by superimposing the flow disturbance caused by ambient shear, relative motion, rotation and the presence of the walls. Using this theoretical method, Leighton & Acrivos analyzed the lift on a stationary sphere in contact with the wall for a linear shear flow [5]. Krishnan & Leighton extended the analysis to predict the lift on a sphere translating and rotating along a wall in a linear shear flow [6]. The lift force variation with wall distance was analyzed by Cherukat & McLaughlin, down to a minimum separation distance of $0.1a$, using this analytical method [7]. Also the extrapolated results for a particle touching the wall agree well with the previous studies. The lift force is usually non-dimensionalized by ${Re_\gamma}^2\mu^2/\rho$ (where ρ is the fluid density), becoming independent of shear for $Re_\gamma \ll 1$ and asymptoting to the value ~ 2 for a non-rotating sphere touching the wall.

The presence of a wall also influences the drag force on a particle under both Stokes and inertial conditions. In wall bounded flows the highest drag is observed when the particle is in contact with wall, and decays rapidly as the distance between the particle and wall increases [8]. Accounting for the velocity field due to both the presence of shear and a wall, Magnaudet presented an additional Faxen type drag component for a sphere in the near wall region [10]. This drag force increases the slip velocity of neutrally buoyant particles near the wall, giving rise to a slip-induced lift force at the wall that causes particles to migrate away from walls. Goldman provides two simple expressions for the drag force acting on a fixed particle in a linear shear flow and on a particle moving in a quiescent fluid in the presence of a wall under Stokes conditions [9]. Further, Magnaudet analyzed the combined effect of slip and shear effects in wall-bounded flows, enabling the authors to deduce the drag on a fixed particle [10].

In contrast to analytical expressions, most numerical studies on wall bounded forces are focused on intermediate Reynolds numbers $Re_\gamma, Re_p \sim 1 - 100$. These studies show a strong influence of shear near the wall on both the drag and lift forces [11, 12]. However, neither these numerical results or the discussed theoretical models have been adequately validated for small but finite inertial conditions $Re \leq O(1)$, particularly in wall-bounded flows.

Hence, in this study, we compute the hydrodynamic forces acting on a non-rotating sphere in a linear flow when the shear Reynolds number is $O(1)$ using a finite-volume solver [13]. Two cases are considered: In the first, the particle moves with the fluid such that the slip velocity is zero ($Re_p = 0$), and any lift forces are due to wall and shear. In the second case, the effect of slip is examined by holding the particle stationary ($Re_p \neq 0$).

Method

Problem Specification

A neutrally buoyant rigid sphere of radius a is suspended in a linear shear fluid flow with the origin of the Cartesian coordinate system located at the center of the sphere (Figure 1). The coordinate unit vectors are $\boldsymbol{e}_x$, $\boldsymbol{e}_y$ and $\boldsymbol{e}_z$. The wall is placed at distance l away from sphere center. The particle is constrained to move in the x direction only, with particle velocity u_p, and is restricted from rotating. Outer boundaries are located at large distances $L(\gg l)$ away from the sphere centre to minimize any secondary boundary effects. For this study l is set to $1.2a$ to obtain the lift and drag forces for a case where the sphere is almost touching the wall. A minimum value for L is numerically established using domain size analysis.

To analyze the effect of slip on the hydrodynamic forces, the two cases are considered. In the absence of relative motion between the particle and the fluid, forces are generated due to only wall and shear effects. To analyze this scenario the particle slip velocity $\boldsymbol{u}_{slip}$ is explicitly set to $\boldsymbol{0}$ in our first case. Note that

the slip is here defined as the particle velocity $\boldsymbol{u}_\mathrm{p}$ relative to the undisturbed fluid velocity $\boldsymbol{u}_\mathrm{f}$ at the particle center ($y = 0$) (Eq.1). In our second case, the particle velocity is set to be 0 to find the forces acting on a fixed particle. For both cases the undisturbed fluid field is considered to be a linear shear flow with a positive shear rate ($\dot{\gamma}$) (Eq.2) and a stationary wall at $z = -l$.

$$\boldsymbol{u}_\mathrm{slip} = \boldsymbol{u}_\mathrm{p} - \boldsymbol{u}_{\mathrm{f\,(y=0)}} \tag{1}$$

$$\boldsymbol{u}_\mathrm{f} = \dot{\gamma}(y + l)\boldsymbol{e}_\mathrm{x} \tag{2}$$

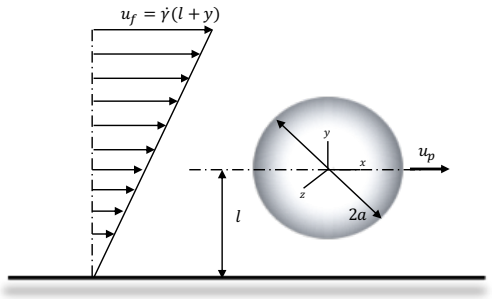

Figure 1: A schematic diagram of a translating sphere of radius a moving at velocity u_p in a wall-bounded linear shear flow

The fluid flow domain is resolved using the steady state dimensional Navier Stokes (N-S) equations in a frame of reference that moves with the particle. This results in a relative fluid velocity $\boldsymbol{u'}$ equal to $\boldsymbol{u} - \boldsymbol{u}_\mathrm{p}$, where $\boldsymbol{u}$ is the local fluid velocity. Hence, the modified steady state N-S equation is solved for $\boldsymbol{u'}$ (Eq.3). The fluid is assumed to be Newtonian with a dynamic viscosity μ and density ρ.

$$\begin{aligned} \boldsymbol{\nabla} \cdot \rho \boldsymbol{u'} &= 0 \\ \boldsymbol{\nabla} \cdot (\rho \boldsymbol{u'} \boldsymbol{u'} + \boldsymbol{\sigma}) &= 0 \end{aligned} \tag{3}$$

The total stress tensor ($\boldsymbol{\sigma} = p\boldsymbol{I} - \boldsymbol{\tau}$) is computed using the fluid pressure (p) and viscous stress tensor ($\boldsymbol{\tau} = -\mu(\boldsymbol{\nabla u'} + \boldsymbol{\nabla u'}^\mathrm{T})$). The boundary conditions (Eq.4) used in the moving frame of reference are:

$$\boldsymbol{u'} = \begin{cases} \dot{\gamma}(y + l)\boldsymbol{e}_\mathrm{x} - \boldsymbol{u}_\mathrm{p} & y = +\infty; x, z = \pm\infty \\ -\boldsymbol{u}_\mathrm{p} & y = -l \\ 0 & |\boldsymbol{r}| = a \end{cases} \tag{4}$$

Here $\boldsymbol{r}$ is a radial displacement vector pointing from the sphere centre to the particle surface.

The forces acting on the particle are evaluated by integrating the total stress contributions around the particle surface A:

$$\boldsymbol{F}_\mathrm{p} = -\int_A \boldsymbol{\sigma} \cdot \boldsymbol{n}\, dA \tag{5}$$

Here $\boldsymbol{n}(= \hat{\boldsymbol{r}})$ is the outward unit normal vector of the particle. The drag ($F_\mathrm{D} = \boldsymbol{F}_\mathrm{p} \cdot \boldsymbol{e}_\mathrm{x}$) and lift ($F_\mathrm{L} = \boldsymbol{F}_\mathrm{p} \cdot \boldsymbol{e}_\mathrm{y}$) are defined as the fluid forces acting on the sphere in $+x$ and $+y$ directions, respectively.

The dimensionless lift and drag coefficients based on the shear are defined as:

$$C_\mathrm{L} = \frac{{F_\mathrm{L}}^*}{Re_\gamma^2} \qquad C_\mathrm{D} = \frac{{F_\mathrm{D}}^*}{Re_\gamma^2} \tag{6}$$

where ${F_\mathrm{L}}^*$ and ${F_\mathrm{D}}^*$ are the forces non-dimensionalised by fluid properties, defined as $F_\mathrm{L}\rho/\mu^2$ and $F_\mathrm{D}\rho/\mu^2$, respectively.

Mesh Development

A nonuniform body fitted structured mesh generated with *gmsh* [14] is employed in the simulation (Figure 2). N_p number of mesh points on each curved side length of a cubed-sphere are used to resolve the sphere shape. This results in $6(N_\mathrm{p} - 1)^2$ cells on the sphere surface. Inflation layers with $(N_\mathrm{d} - 1)$ number of layers and α geometric progression ratio around the sphere are used to capture gradients in velocity occurring near the particle wall (Figure 2). Outer boundaries, except the bottom wall at $-l$, are placed at a distance of L from the sphere centre in all directions. To resolve the far field of the domain (excluding the inflation layers), N_d number of points are used with β geometric progression expanding towards the domain boundaries. The mesh is refined along the wall in the spanwise and normal-to-the-wall direction near the sphere. The total cell count in the mesh is N_t.

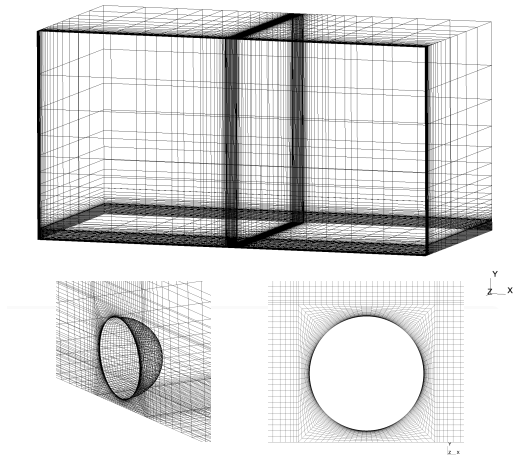

Figure 2: The domain mesh for a particle located at $l/a = 1.2$. Detailed frames show at $z = 0$

Results and Discussion

Domain and Mesh Dependency

The domain size was first tested to determine a suitable choice of L such that the lift force is independent of this parameter. To do this L was gradually increased, maintaining a fixed particle radius and a constant number of total mesh points at $Re_\gamma = 0.004$ and $Re_\mathrm{p} = 0$. The corresponding results are given in Figure 3.

From the results a minimum of $L = 50a$ was selected, capturing the lift coefficient with a $\sim 0.86\%$ difference compared to the largest domain analysed, of $L = 80a$. The selected computational domain size is well within the acceptable range established in previous numerical studies performed for unbounded shear flows at $Re \sim 0.1$ [15, 16]. The boundary layer size around a translating sphere in an unbounded environment is inversely proportional to $\sqrt{Re}$, and hence requires a larger domain size for $Re \ll 1$ [15]. However, for a bounded flow, the wall effect is more significant compared to outer boundary effects, and hence it is reasonable to assume that the selected domain size

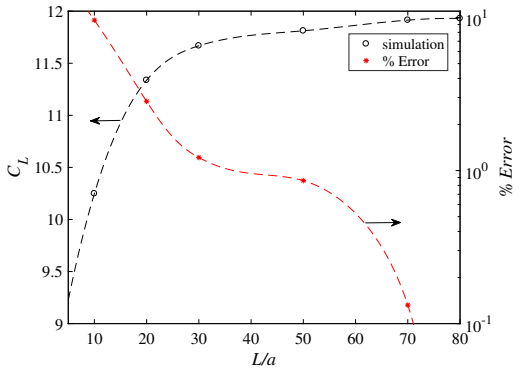

Figure 3: Effect of domain size (L/a) on lift coefficient (C_L) at $Re_\gamma = 0.004$ and $u_\mathrm{p} = 0$. The relative error of C_L compared to the maximum domain size is also presented.

is adequate for all $Re_\gamma \geq 0.004$ by considering the results given above.

Mesh dependency was tested with simulations for a case with the parameters $Re_\mathrm{p} = 0$, $l = 1.2a$ and $L = 50a$. The number of inflation layers around the sphere and the number of cells on the sphere surface were adjusted by varying N_d and N_p respectively. Table 1 summarizes the drag and lift coefficients found for different resolutions with both $Re_\gamma = 0.1$ and 0.01. The percentage difference (ϵ%) relative to the finest mesh results is also given.

Re_γ	Grid		Lift		Drag	
	$N_\mathrm{p}, N_\mathrm{d}$	N_t	C_L	ϵ%	C_D	ϵ%
0.1	15	31556	1.667	2.48	-82.35	1.72
	20	92000	1.639	0.77	-83.41	0.45
	25	158976	1.632	0.32	-83.57	0.26
	30	310500	1.627	-	-83.79	-
0.01	15	31556	2.309	14.89	-833.60	1.65
	20	92000	2.074	3.19	-843.99	0.43
	25	158976	2.058	2.38	-845.51	0.25
	30	310500	2.010	-	-847.61	-

Table 1: Effect of mesh resolution on lift and drag coefficients

According to Table 1, the meshes with $N_\mathrm{p}, N_\mathrm{d} = 20, 25$ and 30 give a relative error between resolutions of less than 1% for $Re_\gamma = 0.1$ and less than 3.2% for $Re_\gamma = 0.01$ for both lift and drag. By considering the accuracy together with computational cost we employed the mesh with $N_\mathrm{p}, N_\mathrm{d} = 25$ and $N_\mathrm{t} = 158976$ in the remainder of the study.

Forces at zero slip

The numerical drag forces for $Re_\gamma = 1 - 0.001$ at $u_\mathrm{slip} = 0$ ($Re_\mathrm{p} = 0$) are given in Figure 4a for a particle close to the wall ($l = 1.2a$). The results are compared with the Goldman [9] and the Magnaudet [10] analytical expressions given for low Reynolds numbers. The data shows the drag force is in the $-x$ direction and increases linearly with the shear Reynolds number. For the selected Re_γ range, both the drag force and its coefficient follow a similar trend predicted by the theoretical models. Simulation results agree well with the Goldman predicted drag forces, but differ by a constant multiplier relative to the Magnaudet results.

The lift force of a zero slip particle close to a wall is shown in Figure 4b. When $Re_\gamma < 0.01$, the numerically computed lift forces agree reasonably well with the previous analytical solutions derived for low Reynolds numbers. C_L is close to the theoretical lift coefficient of ~ 1.9806 for the smallest Re_γ considered, as predicted by Cherukat & McLaughlin [7] when the sphere is close to the wall for low Re_γ. However, as the Re_γ increases, the numerical results deviate significantly from the theoretical results, as inertial effects become more significant. This suggests that the lift coefficient (C_L) at $Re_\mathrm{p} = 0$ requires a shear based inertial correction that is not captured via the analytical models.

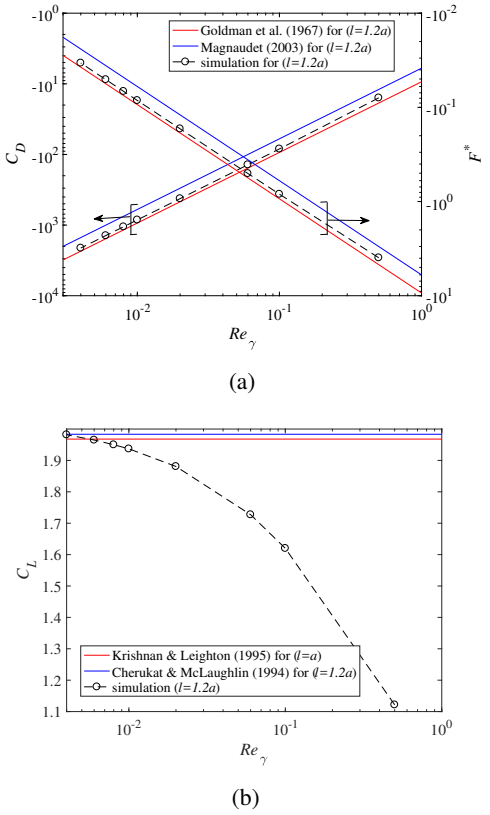

Figure 4: Effect of shear Reynolds number (Re_γ) on a) drag coefficient (C_D) & dimensionless drag force (F^*), and b) lift coefficient (C_L) on a particle near the wall ($l = 1.2a$) for zero slip condition ($Re_\mathrm{p} = 0$). Theoretical drag models - [9] & [10] are evaluated at $l = 1.2a$ and theoretical lift models - [6] & [7] are evaluated at $l = a$ and $l = 1.2a$ respectively.

Forces at non-zero slip

A fixed particle in a sheared flow experiences a u_slip of $-\gamma l$ ($Re_\mathrm{p} \neq 0$). The numerically calculated drag force coefficients given in Figure 5a agree well with previous analytical results given for low Reynolds number [9, 10]. The results show that close to the wall ($l = 1.2a$), the net lateral force acting on the particle is in the $+x$ direction and increases linearly with shear rate. The Goldman model is applicable for Stokes flow and restricted to a fixed particles[9], while the Magnaudet model is applicable for low inertial flows and is presented in a more generalized form combining both shear and slip induced drag components. However, within the region of Re_γ considered, the numerical results agree well with the Goldman drag model [9] compared to the Magnaudet model [10], the latter of which again deviates by a constant multiplier.

The lift coefficient for a fixed particle in a linear shear flow close to the wall ($l = 1.2a$) is given in Figure 5b. For $Re_\gamma \ll 1$, the numerically evaluated C_L asymptotes to ~ 11.8 as $Re_\gamma \to 0$ while the theoretical coefficients are ~ 9.8 [7] for the same particle position. The inconsistency between the numerical and analyti-

cal C_L value for $Re_\gamma \ll 0$ needs further investigation. However, the simulation results show that the lift force coefficient varies significantly with increasing shear Reynolds number, an effect that is again not captured by the theoretical models.

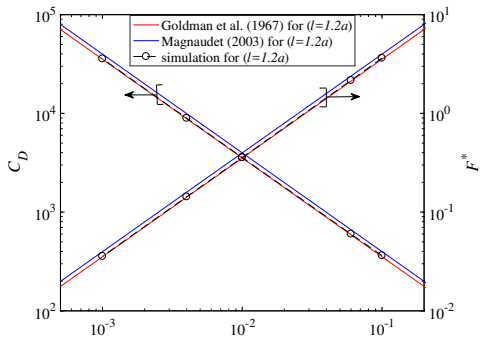

(a)

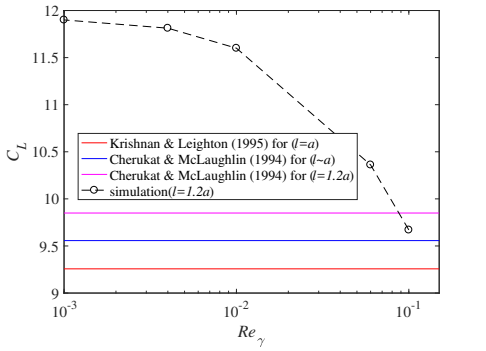

(b)

Figure 5: Effect of shear Reynolds number (Re_γ) on a) drag coefficient (C_D) & dimensionless drag force (F^*), and b) lift coefficient (C_L) on a particle near the wall ($l = 1.2a$) for a fixed particle ($Re_p \neq 0$). Theoretical drag models - [9] & [10] are evaluated at $l = 1.2a$. Theoretical lift models - [6] is evaluated at $l = a$ and [7] is evaluated at $l \sim a$ & $l = 1.2a$ respectively.

Conclusions

The drag and lift forces on a particle close to a wall at finite shear Reynolds numbers Re_γ $(0.001 - 1)$ were numerically evaluated. A domain size of $L = 50a$ was chosen based on a sensitivity analysis. Numerical drag coefficients largely follow the results of the theoretical models derived for $Re_\gamma \ll 1$, even for shear Reynolds numbers $Re_\gamma \sim O(1)$, for both zero and non-zero slip conditions. However, the lift coefficients show a strong dependency on Re_γ with increasing shear rate for both zero slip and non-zero slip cases which is in contrast to the analytical models. Hence, this study suggests that an appropriate shear based inertial correction is required to predict the lift on particles near a wall at finite Reynolds numbers ($Re_\gamma \ll 1$). Assembling a suitable model to capture particle migration near walls in microfluidic devices and blood vessels is the topic of ongoing work.

Acknowledgements

Support from the Australian Research Council and CSL is gratefully acknowledged. Nilanka I. K. Ekanayake acknowledges the support from the Melbourne Research Scholarships program of The Melbourne University.

References

[1] Martel, J. M. and Toner, M., Inertial Focusing in Microfluidics, *An. Rev. of Biomedical Engineering*, **16**, 2014, 371–396.

[2] Leiderman, K., Grow with the flow: a spatial-temporal model of platelet deposition and blood coagulation under flow, *Mathematical Medicine and Biology*, **28**, 2011, 47–84.

[3] Saffman, P. G. T., The lift on a small sphere in a slow shear flow, *J. Fluid Mechanics*, **22**, 1965, 385-400.

[4] Rubinow, S. I. and Keller, J. B., The transverse force on a spinning sphere moving in a viscous fluid, *J. Fluid Mechanics*, **11**, 1961, 447–459.

[5] Leighton, D. and Acrivos, A., The lift on a small sphere touching a plane in the presence of a simple shear flow, *JZeitschrift fÃijr angewandte Mathematik und Physik*, **36**, 1985, 174–178.

[6] Krishnan, G. and Leighton, D., Inertial lift on a moving sphere in contact with a plane wall in a shear flow, *Physics of Fluids*, **7**, 1995, 2538–2545.

[7] Cherukat, P. and McLaughlin, J., The inertial lift on a rigid sphere in a linear shear flow field near a flat wall, *J. Fluid Mechanics*, **263**, 1994, 1–18.

[8] Happel, J. and Brenner, H., Low Reynolds number hydrodynamics. [electronic resource]: with special applications to particulate media, *J. Fluid Mechanics*, **11**, 1961, 447–459.

[9] Goldman, A. J., Cox, R. G. and Brenner, H., Slow viscous motion of a sphere parallel to a plane wall – II Couette flow, *Chemical Engineering Science*, **22**, 1967, 653–660.

[10] Magnaudet, J., Small inertial effects on a spherical bubble, drop or particle moving near a wall in a time-dependent linear flow, *J. Fluid Mechanics*, **485**, 2003, 115–142.

[11] Zeng, L. Najjar, F., Balachandar, S. and Fischer, P., Forces on a finite-sized particle located close to a wall in a linear shear flow, *Physics of Fluids*, **21**, 2009, 033302.

[12] Lee, H. and Balachandar, S., Drag and lift forces on a spherical particle moving on a wall in a shear flow at finite Re, *J. Fluid Mechanics*, **657**, 2010, 89 – 125.

[13] Harvie, D. J. E., An implicit finite volume method for arbitrary transport equations, *ANZIAM Journal. Electronic Supplement*, **52**, 2010, C1126.

[14] Geuzaine C. and Remacle, J. F., Gmsh: a three-dimensional finite element mesh generator with built-in pre- and post-processing facilities., *International Journal for Numerical Methods in Engineering*, **79**, 2009, 1309 – 1331.

[15] Dandy, D. S. and Dwyer, Harry, A., A sphere in shear flow at finite Reynolds number: effect of shear on particle lift, drag, and heat transfer, *J. of Fluid Mechanics*, **216**, 1990, 381–410.

[16] Cherukat, P. and McLaughlin, J. B. and Dandy, D. S., A computational study of the inertial lift on a sphere in a linear shear flow field, *Int. Jou. of Multiphase Flow. Electronic Supplement*, **25**, 1999, 15–33.